Materials Advances

ROYAL SOCIETY OF CHEMISTRY

PAPER

View Article Online
View Journal | View Issue

Cite this: *Mater. Adv.*, 2022, 3, 4932

Black single crystals of lead-free perovskite $Cs_2Ag(Bi:Ru)Br_6$ with an intermediate band†

Zehao Zhang,‡[a] Ganghong Liu,‡[a] Wenhui Guo,‡[a] Xiangdong Li,[a] Yuqing Zhang,[a] Cuncun Wu,[b] Bo Qu,*[a] Jun-jie Shi,[a] Zhijian Chen*[a] and Lixin Xiao*[a]

Received 6th March 2022,
Accepted 6th May 2022

DOI: 10.1039/d2ma00264g

rsc.li/materials-advances

The toxicity of lead halide perovskites hinders their application in optoelectronics. Lead-free $Cs_2AgBiBr_6$ is regarded as a promising candidate due to its excellent photoelectric properties. However, its excessively wide band gap limits its absorption in the visible region. Herein, we incorporated the transition metal Ru^{3+} into $Cs_2AgBiBr_6$ and obtained black single crystals by a hydrothermal method. The absorption edge was extended from ~660 nm to the near-infrared region (~1200 nm). When 1.8% of Ru was doped, the double perovskite structure was still maintained and the lattice shrank since some Bi^{3+} was replaced by smaller Ru^{3+}. Theoretical calculation indicates that after Ru-doping, a new intermediate band was generated inside the pristine band gap of $Cs_2AgBiBr_6$ as experimentally confirmed by Valence Band X-ray Photoelectron Spectroscopy. The intermediate band lies below the Fermi surface and is mainly dominated by the Ru-d orbital. Moreover, with the fabrication of a near-infrared (NIR) photodetector, a NIR response from the Ru-doped $Cs_2AgBiBr_6$ was realized. This work provides an effective way of regulating the energy band structure of $Cs_2AgBiBr_6$ and extends the application of lead-free perovskites for optoelectronic devices, such as NIR detectors and intermediate band solar cells.

1. Introduction

Lead halide perovskites have rapidly advanced in the field of optoelectronics due to their adjustable bandgaps,[1] long carrier diffusion length,[2] high defect tolerance[3] and low-cost process.[4] However, the toxicity of water-soluble Pb^{2+} hinders their broad application.[5] The research of low-toxicity elements to replace Pb has become more attractive for the development of next generation perovskites. The Sn-based perovskite that uses Sn^{2+} to replace Pb^{2+} exhibits extremely good photoelectric properties, but Sn^{2+} is easily oxidized to Sn^{4+}.[6,7] In addition, most of the perovskite derivatives including 2D $A_3B_2^{3+}X_9$,[8] 0D $A_2B^{4+}X_6$[9] and 0D $A_3B_2^{3+}X_9$[10] (A: Cs^+, MA^+, FA^+; B: metal ions; X: Cl^-, Br^-, I^-) have slightly worse optoelectronic properties, due to lower electronic dimensions, large effective mass and poor carrier transport capabilities.[11–14] Recently, 3D double perovskites ($A_2B^+B^{3+}X_6$), especially $Cs_2AgBiBr_6$, are considered to be promising candidates for photovoltaics[15,16] and detectors,[17,18] due to their intrinsic thermodynamic stability and small carrier effective masses.[19] However, compared with lead halide perovskites, the excessively wide band gap of $Cs_2AgBiBr_6$[15,20] provides inferior light absorption, which severely limits its application in the photovoltaic field. Therefore, exploring effective strategies to expand its optical absorption is crucial to the development of highly efficient photovoltaics and detectors.

Element doping is an effective method to modulate the band structure of a semiconductor. According to previous reports,[21,22] however, it is not successful in achieving a narrower band gap through A-site or X-site doping. Therefore, more research groups focus on B-site doping. Karunadasa *et al.* reduced the band gap of $Cs_2AgBiBr_6$ through Tl-doping, and the indirect band gap reaches about 1.4 eV (~890 nm).[23] However, Tl is highly toxic. In their subsequent work, non-toxic but unstable Sn^{2+} was selected as the doping element, and the band gap of the double perovskite was also significantly reduced, with the indirect band gap reaching 1.48 eV (~840 nm).[24] In addition, there are some reports that Sb-doping can also reduce the band gap to a certain extent.[25,26] Gao *et al.* successfully broadened the absorption edge of $Cs_2AgBiBr_6$ to the near-infrared (NIR) region to ~860 nm *via*

[a] *State Key Laboratory for Mesoscopic Physics and Department of Physics, Peking University, Beijing 100871, China. E-mail: bqu@pku.edu.cn, zjchen@pku.edu.cn, lxxiao@pku.edu.cn*
[b] *School of Materials Science and Engineering, State Key Laboratory of Reliability and Intelligence of Electrical Equipment, Hebei University of Technology, Tianjin 300130, China*

† Electronic supplementary information (ESI) available: The experimental details, the data of ICP-OES, lattice constants and the additional figures of XRD patterns. Simulated lattice structure used in calculations and the partial density of states of Ru-s/p/d. See DOI: https://doi.org/10.1039/d2ma00264g

‡ These authors contributed equally.

Cu-doping.[27] However, according to their experimental results, Cu cannot enter the crystal lattice of $Cs_2AgBiBr_6$, and it is also difficult to change the band structure of the double perovskite. The shift of the absorption edge after doping is due to the introduction of sub-bandgap states. Their group also successfully incorporated Fe^{3+} into $Cs_2AgInCl_6$ to realize the red shift of the absorption edge to about 800 nm.[28] In addition, they also successfully incorporated Fe^{3+} into $Cs_2AgBiBr_6$ and developed new spintronic materials.[29] It is worth noting that based on their sample photos, the original red single crystal changed to black after Fe^{3+} doping and its absorption tailing reaches ~800 nm.[29] Searching for a stable and non-toxic element to effectively extend the absorption of $Cs_2AgBiBr_6$ remains challenging.

In previous work,[30] we successfully incorporated Fe into $Cs_2AgBiBr_6$ to extend the absorption to the NIR region. As a congener of Fe, Ru has a wide application in dye-sensitized solar cells (DSSC), *e.g.*, N719 dye is a Ru complex.[31] Gu *et al.* reported on the incorporation of Ru^{3+} into $Cs_3Bi_2I_9$ to replace partial Bi^{3+} and experimentally confirmed the feasibility of Ru^{3+} replacing Bi^{3+} in perovskite crystals.[32] Although Fe and Ru, from the same family, have similar characteristics, they differ in electron configuration (Fe: $3d^64s^2$, Ru: $4d^75s^1$), electronegativity (Ru: 2.2, Fe: 1.8) and ion size.[33] To investigate the doping thermodynamic process, we studied the Ru-doping effect on double perovskite. In this work, we successfully doped Ru^{3+} into $Cs_2AgBiBr_6$ to partially replace Bi^{3+} to form $Cs_2Ag(Bi:Ru)Br_6$ and obtained black single crystals. Benefiting from the similar properties, $Cs_2Ag(Bi:Ru)Br_6$ has similar characteristics to the Fe-doped one. The absorption edge of $Cs_2Ag(Bi:Ru)Br_6$ was extended to ~1200 nm and the lattice shrunk. Theoretical calculation indicates that after the introduction of Ru^{3+}, a new intermediate band, which was mainly dominated by the Ru-d orbital, was generated inside the pristine band gap. Due to the different electronegativity and ionic size of Fe and Ru, the bond lengths of Ru–Br and Fe–Br in metal bromide are different, which are 2.5 Å and 2.4 Å, respectively. Meanwhile, the bond length of Bi–Br is 2.9 Å. (Crystal data is referenced from mp-22892, mp-752602 and mp-23232, MaterialsProject). Compared with Fe–Br, the bond length of Ru–Br is closer to Bi–Br, so Ru can more easily replace Bi in the lattice than Fe. Therefore, doping can be achieved with Ru at a lower concentration in the precursor. Furthermore, the intermediate band lies below the Fermi surface. Finally, we observed experimentally the existence of the intermediate band by Valence Band X-ray Photoelectron Spectroscope (VB-XPS), revealing that the intermediate band is located at a position about 1 eV above the original valence band maximum (VBM). $Cs_2Ag(Bi:Ru)Br_6$ has the potential to be applied in intermediate band solar cells, which may break the Shockley–Queisser limit.[34] In addition, a NIR response was observed for $Cs_2Ag(Bi:Ru)Br_6$ single crystal, indicating its potential application in NIR detection and other optoelectronic fields.

2. Results and discussion

Ru-doped $Cs_2AgBiBr_6$ single crystals (shown in Fig. 1a) were synthesized by a hydrothermal method. The doping level of Ru

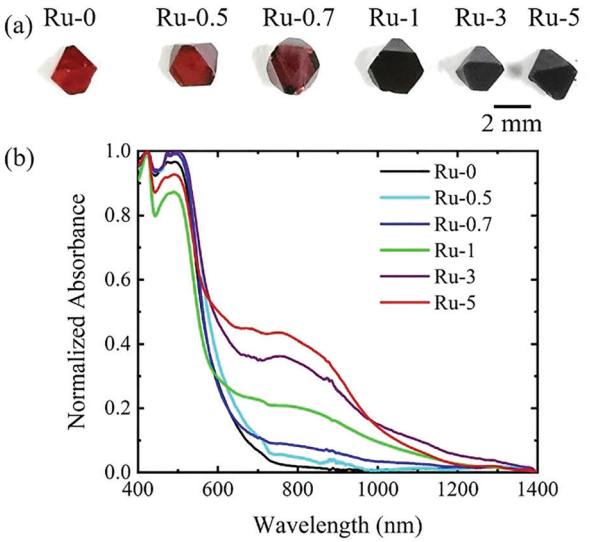

Fig. 1 (a) Photographs and (b) the normalized absorption of the samples.

was tuned by different amounts of $RuBr_3$ in the precursor solution. We named samples according to the molar ratio of Ru (Ru/(Ru + Bi)) in the precursor, *e.g.*, Ru-5 means Ru/(Ru + Bi) × 100% = 5%. And Ru-0 is pristine $Cs_2AgBiBr_6$ without Ru-doping. It can be clearly seen that Ru doping causes the single crystals to gradually change their colour from red to black, *i.e.*, Ru-0.5, Ru-0.7, Ru-1, Ru-3 and Ru-5, as shown in Fig. 1. The molar ratio of Ru in the precursor solution does not represent the specific ratio of Ru in the resultant single crystal. Therefore, we used inductively coupled plasma optical emission spectrometry (ICP-OES) to determine the specific molar ratio of Ru in the single crystal. The data is shown in Table S1 (ESI†). Since Ag and Br will form AgBr precipitates during the digestion process, the content of Ag and Br is not measured. This result indicates that Ru actually replaced about 0.30%, 1.07% and 1.85% of Bi in Ru-1, Ru-3 and Ru-5, respectively. Since the concentration of Ru-doping in Ru-0.7 is ultra-low, the actual content of Ru is hardly measured. According to the absorption spectrum (Fig. 1b), the absorption edge of Ru-0 is at about 630 nm, which is consistent with the previous reports.[15,20] After introducing Ru-dopants, the absorption spectra of the samples changed significantly. The absorption edges of Ru-3 and Ru-5 were very close, as shown in Fig. S1 (ESI†). For Ru-5, the new absorption edge was located close to 1200 nm.

However, by characterizing the PL spectrum of the sample (Fig. S2, ESI†), it is found that the peak position was basically unchanged. However, after Ru doping, the PL peaks of the samples were obviously weakened, indicating that the doping brought defects and led to the enhancement of non-radiative recombination.

XRD measurement was carried out to study the effect of Ru doping on the crystal structure of the double perovskite. According to the XRD patterns (Fig. 2), the crystals of Ru-1, 3 and 5 have a double perovskite structure (Fig. 2a), and their diffraction peaks (220) shift towards a larger angle than that of Ru-0 (Fig. 2b). According to the Bragg equation, a larger

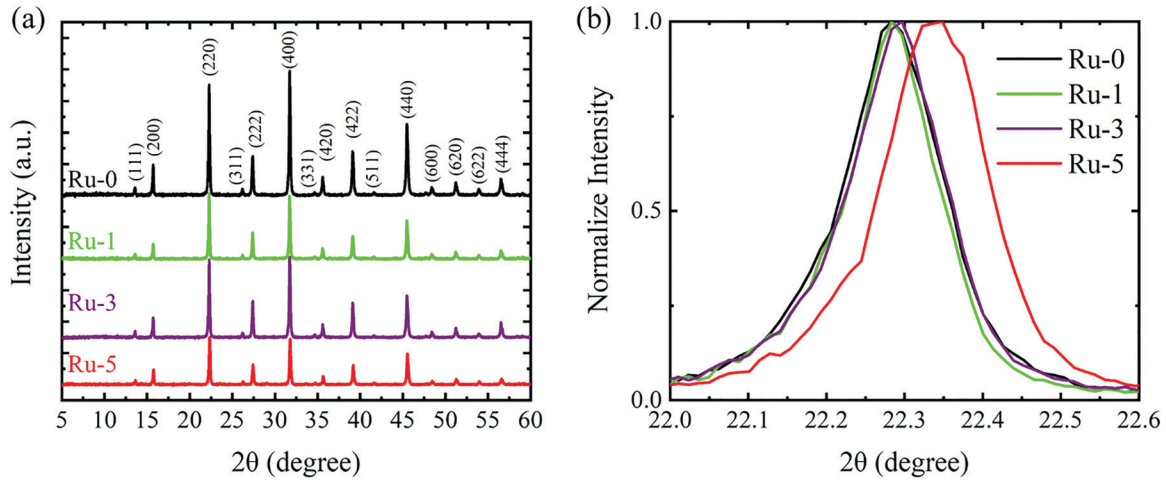

Fig. 2 (a) XRD patterns of $Cs_2Ag(Bi:Ru)Br_6$. (b) An expansion of the diffraction peak of (220).

diffraction angle means a smaller lattice constant. This lattice shrink phenomenon is caused by the partial replacement of Bi^{3+} (1.03 Å) by the smaller Ru^{3+} (0.68 Å).[33] As the doping concentration increases, the lattice shrinkage is enhanced. The specific lattice constants are shown in Table S2 (ESI†). Ru-5 is the sample with the largest doping concentration we can get, and thus the following discussion will focus on Ru-5.

To further clarify the effect of Ru-doping on the band structure of the double perovskite and to find out the reason for the change in the absorption spectra, we carried out DFT calculations to study the energy band structure. The simulated crystal structure of $Cs_2Ag(Bi:Ru)Br_6$ is shown in Fig. S3 (ESI†). The calculated lattice constant of (11.292 Å) $Cs_2AgBiBr_6$ is consistent with the experimental one (11.280 Å), as listed in Table S2 (ESI†). And the experimental and calculated XRD spectra are accordant (Fig. S4, ESI†). The aforementioned results ensure the calculating precision generally. To reduce computational cost, we constructed some small models that were sufficient to describe the effects of Ru doping. For $Cs_2AgBiBr_6$, we observed bandgap underestimation (Fig. 3a) which was consistent with previous reports.[24] Fig. 3b shows that the calculated band gap of $Cs_2AgBiBr_6$ is reduced after 25% Ru-doping, which stems from the huge effect on the band structure of Ru. A new energy band appeared after Ru doping, which we named the intermediate band. Obviously, the intermediate band below the Fermi level is dominated by Ru-d orbitals mainly (Fig. S5, ESI†), which causes additional transition channels from the intermediate band to the unoccupied bands. The intermediate band is quite flat, which would lead to high photo-carrier effective mass and small mobility, *i.e.*, the transport property of $Cs_2AgBiBr_6$ weakens after Ru-doping. To further discuss the effect of Ru-doping concentration on the band structure of $Cs_2Ag(Bi:Ru)Br_6$, we calculate the band structures of $Cs_2Ag(Bi_1Ru_0)Br_6$, $Cs_2Ag(Bi_{0.75}Ru_{0.25})Br_6$, $Cs_2Ag(Bi_{0.5}Ru_{0.5})Br_6$ and $Cs_2Ag(Bi_{0.25}Ru_{0.75})Br_6$, as exhibited in Fig. S6 (ESI†). The energy difference between the intermediate band and CBM decreased with the increase of the Ru doping concentration. The energy level of the intermediate band remains

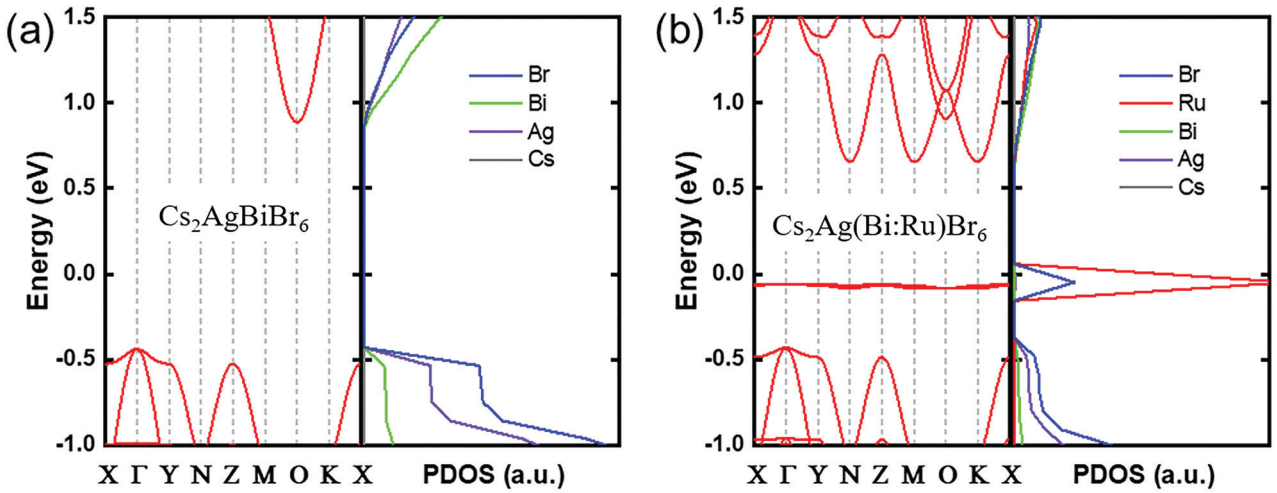

Fig. 3 The calculated band structures and partial density of states (PDOS) of (a) $Cs_2AgBiBr_6$ and (b) $Cs_2Ag(Bi_{0.75}Ru_{0.25})Br_6$. The Fermi level is set at 0 eV.

almost constant near the Fermi level for various Ru-doping concentrations. A similar phenomenon was also found in our previous report on Fe-doped $Cs_2AgBiBr_6$.[30] Therefore, we have abundant proof that there is also such an intermediate band in $Cs_2Ag(Bi:Ru)Br_6$, which lead to absorption in NIR region.

VB-XPS was used to confirm experimentally the influence of Ru-doping on the band structure (Fig. 4). The bands with binding energy less than 8 eV show obvious changes (Fig. 4b). In the case of $Cs_2AgBiBr_6$, two signal peaks with binding energies of 3.91 eV and 5.64 eV were observed, respectively (Fig. 4c). There are three signal peaks in the spectrum of Ru-5, corresponding to three energy levels with binding energies of 2.74 eV, 3.72 eV and 5.54 eV, respectively (Fig. 4d). Therefore, the intermediate band after Ru-doping was experimentally confirmed at the position of ~1 eV above the original VBM. It is the intermediate band that causes the absorption edge to redshift towards the NIR region. Materials with intermediate bands have been proposed to fabricate intermediate band solar cells, which may break the Shockley-Queisser efficiency limitation.[34]

The transition process of Ru-doped samples is shown in Fig. 5a. Process (1) is the transition from the VBM to the CBM of $Cs_2AgBiBr_6$ constituting the visible part of the absorption spectrum, and process (2) is the transition from the intermediate band to the CBM constituting the near-infrared part of the absorption spectrum. The data of VBM and CBM are referenced from our previous work.[15] Motivated by the absorption of Ru-doping samples in the NIR region, we fabricated the device by evaporating Au electrodes on a single crystal of Ru-5. For comparison, a device based on Ru-0 was also manufactured. The schematic diagram of the devices is shown in Fig. 5b. The Volt-Ampere characteristic curves of the devices are shown in Fig. 5c and d. It can be clearly observed that the dark current of the devices after Ru-doping is significantly reduced and there is a clear photoelectric response at 980 nm (the longest wavelength of light source available in our lab). However, the $Cs_2AgBiBr_6$ device has no photoelectric conversion capability for 980 nm, but it is suitable for UV and visible light detection as reported in our previous work.[17] Thus, $Cs_2Ag(Bi:Ru)Br_6$ shows potential for a lead-free perovskite infrared detector.

3. Conclusion

Similar to Fe doping, we have successfully obtained black single crystals and extended the absorption edge of $Cs_2AgBiBr_6$ to the

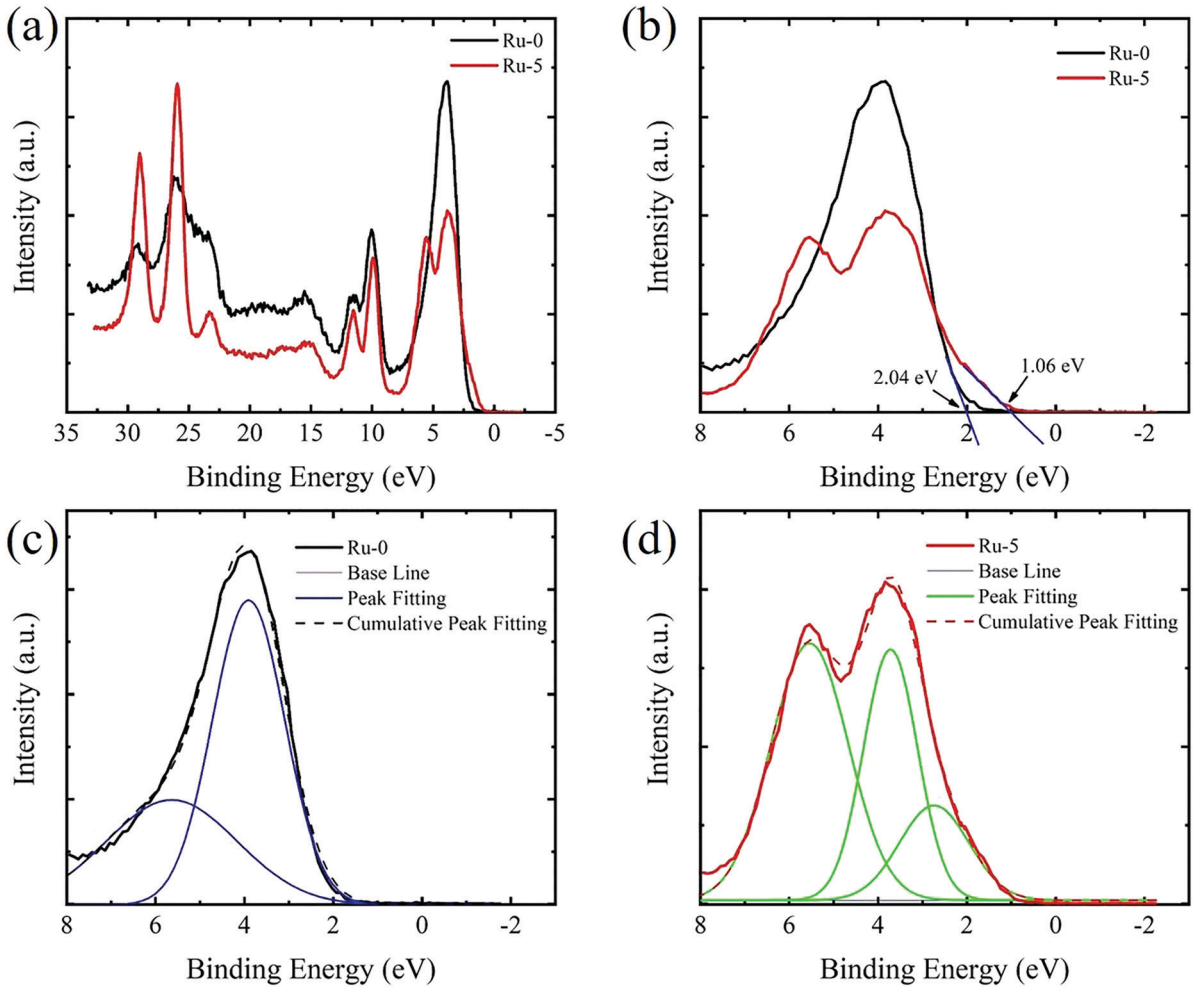

Fig. 4 (a) The VB-XPS spectrum of Ru-0 and Ru-5. (b) An expansion of the region with binding energy below 8 eV. The multi-peak fitting of the spectra of (c) Ru-0 and (d) Ru-5.

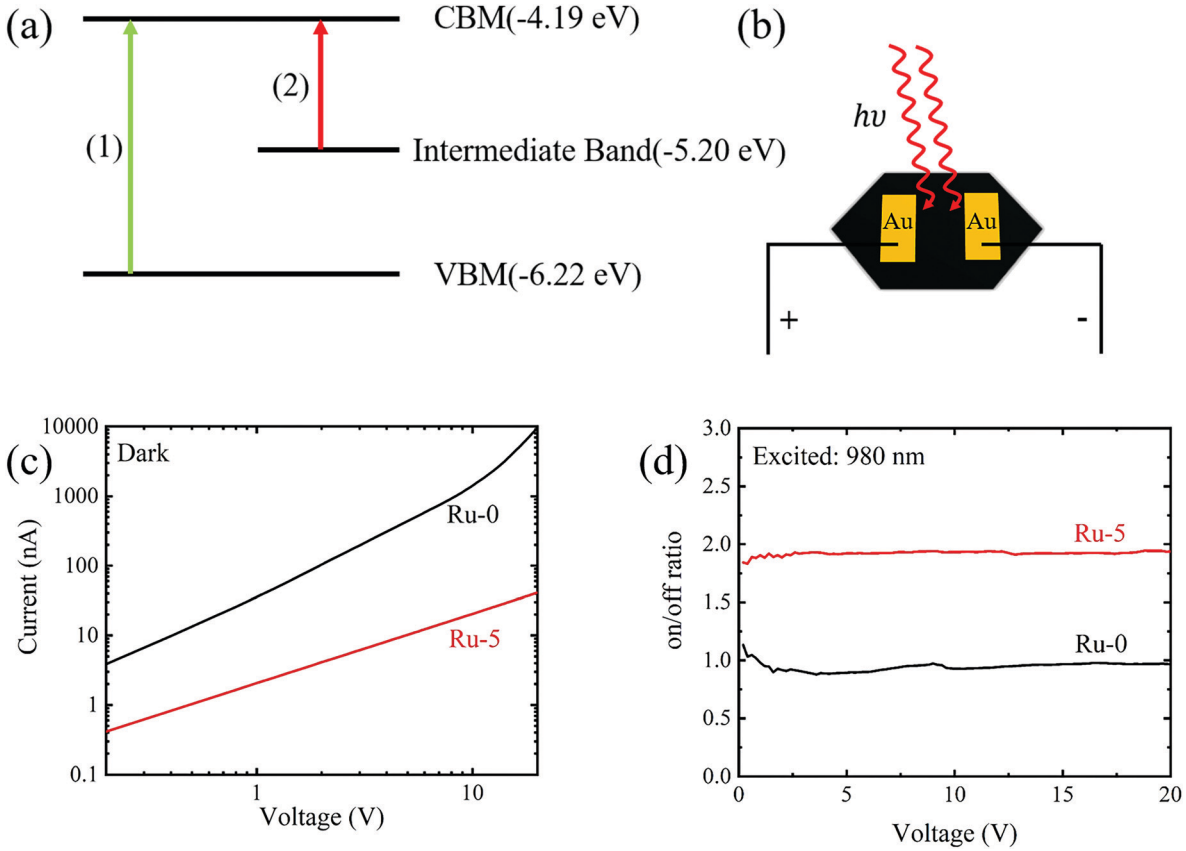

Fig. 5 (a) Schematic illustration of the transition process of the Ru-doping samples. (b) Schematic diagram of the devices. (c) The Volt-Ampere characteristic curves of the devices under dark conditions. (d) On/off ratios of the devices under 980 nm.

NIR region (~1200 nm) with an intermediate band *via* incorporating transition metal Ru. The partial substitution of Bi by Ru (<2 mol.%) led to the crystal lattice shrinking. The intermediate band, mainly dominated by Ru-d orbitals, resulted in the absorption redshift. However, due to the difference of Ru and Fe, Ru is more easily doped into $Cs_2AgBiBr_6$, and the position of the intermediate band is below the Fermi surface. Moreover, we experimentally confirmed that the intermediate band was located at ~1 eV above the original VBM of $Cs_2AgBiBr_6$ by VB-XPS. The confirmed NIR photoelectric response implied the potential application for intermediate band solar cells and NIR photodetectors. Our work provides an efficient method to reduce the band gap of lead-free perovskites, and extending the optoelectronic response to the NIR region.

4. Experimental Methods

The experimental section is provided in the ESI.†

Author contributions

Zehao Zhang, Ganghong Liu and Wenhui Guo contributed equally.

Conflicts of interest

The authors declare no competing financial interest.

Acknowledgements

This work was supported by the National Natural Science Foundation of China (12174013, 61935016, 52173153, 12074011, 62104059). The DFT calculations are supported by the High-performance Computing Platform of Peking University.

References

1 J. H. Noh, S. H. Im, J. H. Heo, T. N. Mandal and S. I. Seok, *Nano Lett.*, 2013, **13**, 1764–1769.
2 G. Xing, N. Mathews, S. Sun, S. S. Lim, Y. M. Lam, M. Grätzel, S. Mhaisalkar and T. C. Sum, *Science*, 2013, **342**, 344.
3 C. Ran, J. Xu, W. Gao, C. Huang and S. Dou, *Chem. Soc. Rev.*, 2018, **47**, 4581–4610.
4 X. Li, D. Bi, C. Yi, J.-D. Décoppet, J. Luo, S. M. Zakeeruddin, A. Hagfeldt and M. Grätzel, *Science*, 2016, **353**, 58.
5 A. Babayigit, A. Ethirajan, M. Muller and B. Conings, *Nat. Mater.*, 2016, **15**, 247–251.

6 C. Wang, F. Gu, Z. Zhao, H. Rao, Y. Qiu, Z. Cai, G. Zhan, X. Li, B. Sun, X. Yu, B. Zhao, Z. Liu, Z. Bian and C. Huang, *Adv. Mater.*, 2020, **32**, 1907623.
7 N. K. Noel, S. D. Stranks, A. Abate, C. Wehrenfennig, S. Guarnera, A.-A. Haghighirad, A. Sadhanala, G. E. Eperon, S. K. Pathak, M. B. Johnston, A. Petrozza, L. M. Herz and H. J. Snaith, *Energy Environ. Sci.*, 2014, **7**, 3061–3068.
8 B. Saparov, F. Hong, J.-P. Sun, H.-S. Duan, W. Meng, S. Cameron, I. G. Hill, Y. Yan and D. B. Mitzi, *Chem. Mater.*, 2015, **27**, 5622–5632.
9 B. Lee, A. Krenselewski, S. I. Baik, D. N. Seidman and R. P.-H. Chang, *Sustainable Energy Fuels*, 2017, **1**, 710–724.
10 B.-W. Park, B. Philippe, X. Zhang, H. Rensmo, G. Boschloo and E. M.-J. Johansson, *Adv. Mater.*, 2015, **27**, 6806–6813.
11 W. Ning and F. Gao, *Adv. Mater.*, 2019, **31**, 1900326.
12 C. Wu, Q. Zhang, G. Liu, Z. Zhang, D. Wang, B. Qu, Z. Chen and L. Xiao, *Adv. Energy Mater.*, 2020, **10**, 1902496.
13 Z. Xiao, W. Meng, J. Wang, D. B. Mitzi and Y. Yan, *Mater. Horiz.*, 2017, **4**, 206–216.
14 Z. Jin, Z. Zhang, J. Xiu, H. Song, T. Gatti and Z. He, *J. Mater. Chem. A*, 2020, **8**, 16166–16188.
15 C. Wu, Q. Zhang, Y. Liu, W. Luo, X. Guo, Z. Huang, H. Ting, W. Sun, X. Zhong, S. Wei, S. Wang, Z. Chen and L. Xiao, *Adv. Sci.*, 2018, **5**, 1700759.
16 W. Ning, F. Wang, B. Wu, J. Lu, Z. Yan, X. Liu, Y. Tao, J.-M. Liu, W. Huang, M. Fahlman, L. Hultman, T. C. Sum and F. Gao, *Adv. Mater.*, 2018, **30**, 1706246.
17 C. Wu, B. Du, W. Luo, Y. Liu, T. Li, D. Wang, X. Guo, H. Ting, Z. Fang, S. Wang, Z. Chen, Y. Chen and L. Xiao, *Adv. Opt. Mater.*, 2018, **6**, 1800811.
18 M. Keshavarz, E. Debroye, M. Ottesen, C. Martin, H. Zhang, E. Fron, R. Küchler, J. A. Steele, M. Bremholm, J. Van de Vondel, H. I. Wang, M. Bonn, M. B.-J. Roeffaers, S. Wiedmann and J. Hofkens, *Adv. Mater.*, 2020, **32**, 2001878.
19 X.-G. Zhao, J.-H. Yang, Y. Fu, D. Yang, Q. Xu, L. Yu, S.-H. Wei and L. Zhang, *J. Am. Chem. Soc.*, 2017, **139**, 2630–2638.
20 A. H. Slavney, T. Hu, A. M. Lindenberg and H. I. Karunadasa, *J. Am. Chem. Soc.*, 2016, **138**, 2138–2141.
21 Z. Zhang, C. Wu, D. Wang, G. Liu, Q. Zhang, W. Luo, X. Qi, X. Guo, Y. Zhang, Y. Lao, B. Qu, L. Xiao and Z. Chen, *Org. Electron.*, 2019, **74**, 204–210.
22 Z. Yu, Y. Wenjin, Z. Lixiu, W. Cuncun, X. Lixin and D. Liming, *J. Semicond.*, 2021, **42**, 120202–120203.
23 A. H. Slavney, L. Leppert, D. Bartesaghi, A. Gold-Parker, M. F. Toney, T. J. Savenije, J. B. Neaton and H. I. Karunadasa, *J. Am. Chem. Soc.*, 2017, **139**, 5015–5018.
24 K. P. Lindquist, S. A. Mack, A. H. Slavney, L. Leppert, A. Gold-Parker, J. F. Stebbins, A. Salleo, M. F. Toney, J. B. Neaton and H. I. Karunadasa, *Chem. Sci.*, 2019, **10**, 10620–10628.
25 K.-z Du, W. Meng, X. Wang, Y. Yan and D. B. Mitzi, *Angew. Chem., Int. Ed.*, 2017, **56**, 8158–8162.
26 E. M. Hutter, M. C. Gélvez-Rueda, D. Bartesaghi, F. C. Grozema and T. J. Savenije, *ACS Omega*, 2018, **3**, 11655–11662.
27 F. Ji, Y. Huang, F. Wang, L. Kobera, F. Xie, J. Klarbring, S. Abbrent, J. Brus, C. Yin, S. I. Simak, I. A. Abrikosov, I. A. Buyanova, W. M. Chen and F. Gao, *Adv. Funct. Mater.*, 2020, **30**, 2005521.
28 F. Ji, F. Wang, L. Kobera, S. Abbrent, J. Brus, W. Ning and F. Gao, *Chem. Sci.*, 2021, **12**, 1730–1735.
29 W. Ning, J. Bao, Y. Puttisong, F. Moro, L. Kobera, S. Shimono, L. Wang, F. Ji, M. Cuartero, S. Kawaguchi, S. Abbrent, H. Ishibashi, R. De Marco, A. Bouianova Irina, A. Crespo Gaston, Y. Kubota, J. Brus, Y. Chung Duck, L. Sun, M. Chen Weimin, G. Kanatzidis Mercouri and F. Gao, *Sci. Adv.*, 2020, **6**, eabb5381.
30 G. Liu, Z. Zhang, C. Wu, Y. Zhang, X. Li, W. Yu, G. Yao, S. Liu, J.-J. Shi, K. Liu, Z. Chen, L. Xiao and B. Qu, *Adv. Funct. Mater.*, 2021, 2109891.
31 J. M. Kroon, N. J. Bakker, H. J.-P. Smit, P. Liska, K. R. Thampi, P. Wang, S. M. Zakeeruddin, M. Grätzel, A. Hinsch, S. Hore, U. Würfel, R. Sastrawan, J. R. Durrant, E. Palomares, H. Pettersson, T. Gruszecki, J. Walter, K. Skupien and G. E. Tulloch, *Prog. Photovoltaics Res. Appl.*, 2007, **15**, 1–18.
32 J. Gu, G. Yan, Y. Lian, Q. Mu, H. Jin, Z. Zhang, Z. Deng and Y. Peng, *RSC Adv.*, 2018, **8**, 25802–25807.
33 R. D. Shannon, *Acta Crystallogr., Sect. A: Cryst. Phys., Diffr., Theor. Gen. Crystallogr.*, 1976, **32**, 751–767.
34 A. S. Brown and M. A. Green, *J. Appl. Phys.*, 2003, **94**, 6150–6158.